SUPPLEMENT TO THE *WELDING JOURNAL*, OCTOBER 2002
Sponsored by the American Welding Society and the Welding Research Council

Aging of Brazed Joints — Interface Reactions in Base Metal/Filler Metal Couples — Part 1: Low-Temperature Ag-Cu-Ti Filler Metal

A study of filler metal/base metal interactions was conducted on brazements of alloys used in advanced heat engines

BY P. T. VIANCO, F. M. HOSKING, J. J. STEPHENS, C. A. WALKER, M. K. NEILSEN, S. J. GLASS, AND S. L. MONROE

ABSTRACT. The effects of aging were examined for brazed joints made with 63.3Ag-35.1Cu-1.6Ti filler metal and Thermo-Span™ (24.5Ni-29.0Co-5.5Cr-4.8Nb-(Si, Ti, Al)-bal. Fe) and Inconel™ 718 (55Ni-21Cr-5.5 (Nb+Ti)-3.3Mo-bal. Fe) base metals. In a companion study, the aging of 81Au-17.5Ni-1.5Ti brazed joints made of Thermo-Span™ and AISI Type 347 stainless steel (18Cr-11Ni-2Mn-1Si-(Ta, Nb)-0.08C-bal. Fe) was examined, the results of which will be presented in Part 2. Excellent wetting and spreading was shown by the Ag-Cu-Ti filler metal on both substrates, as determined by contact angle measurements. The Thermo-Span™/Ag-Cu-Ti couple interface was comprised of two sublayers having the same composition, 90[(Fe, Ni, Co, Cu)$_2$(Nb, Ti, Si, Cr)] 10 Ag, which were separated by a Ag-rich layer. Aging reduced the interface structure to a single phase having the composition (Fe, Ni, Co, Cu)$_2$(Nb, Ti, Si, Cr). The interface reaction zone in the as-fabricated Inconel™ 718/Ag-Cu-Ti couples contained two sublayers having the composition (Fe,Ni,Cu)$_3$(Ti,Cr,Nb,Mo)$_2$ and (Fe,Ni,Cu)$_2$(Ti,Cr,Nb,Mo). Solid-state aging caused the overall reaction layer to thicken and the composition of the second sublayer to change to (Fe,Ni,Cu)$_7$(Ti,Cr,Nb,Mo)$_3$. The bend bar fracture strengths measured for Thermo-Span™/Ag-Cu-Ti and Inconel™ 718/Ag-Cu-Ti couples were not significantly affected by the solid-state aging processes.

P. T. VIANCO (ptvianc@sandia.gov), *F. M. HOSKING, J. J. STEPHENS, C. A. WALKER, M. K. NEILSEN, S. J. GLASS, and S. L. MONROE are with Sandia National Laboratories, Albuquerque, N.Mex.*

Introduction

Advanced heat engines are being developed that operate at higher combustion temperatures for improved fuel efficiency. Ceramic components and, in particular, engineered ceramics such as silicon nitride (Si_3N_4) and partially stabilized zirconia (PSZ) can provide the necessary physical and mechanical properties that will allow for higher operating temperatures in future power plants (Refs. 1–3).

However, the construction of monolithic engine structures from engineered ceramics is not presently feasible. Metal and alloy parts are still required for many components, not only because they have suitable physical and mechanical properties but also because they support cost-effective manufacturing of the engine unit.

KEY WORDS

Long-Term Aging
Brazing
Brazement
Ceramic
Heat Engines
Inconel™
Thermo-Span™

Consequently, the use of metal and ceramic components in advanced heat engines will require the development of suitable joining techniques for all three categories: 1) metal-to-metal, 2) ceramic-to-ceramic, and 3) metal-to-ceramic.

The foremost challenge of making metal-to-ceramic joints rests with accommodating the thermal expansion mismatch between metal substrate materials and the engineered ceramics, and minimizing the resulting residual stresses. Ceramics and glasses tend to have relatively low thermal expansion coefficients. For example, Al_2O_3 and the engineered ceramic Si_3N_4 have thermal expansion coefficients of 7–9 ppm/°C (4–5 ppm/°F) and 3.2–3.5 ppm/°C (1.8–1.9 ppm/°F), respectively (Refs. 4–6). Several metal alloys have been developed to have a reduced thermal expansion coefficient; the traditional trade names and compositions include Kovar™ (Fe-29Ni-17Co), Invar 36™ (Fe-36Ni), and Alloy 42™ (Fe-40.5Ni) having coefficients of 6.2 ppm/°C (3.4 ppm/°F) averaged over 25° to 500°C (77° to 932°F), 7.2 ppm/°C (3.4 ppm/°F) for 25° to 371°C (77° to 700°F), and 8.1 ppm/°C (4.5 ppm/°F) for 25° to 500°C (77° to 932°F), respectively (Refs. 7, 8).

The mechanical performance of the brazed joint also depends strongly on its microstructure. The joint has three major components: 1) the filler metal region, 2) the interface(s) between the filler metal and the base metal, and 3) the base metal. The postprocess microstructure of the joint is a function of the filler metal and base metal compositions, as well as the so-

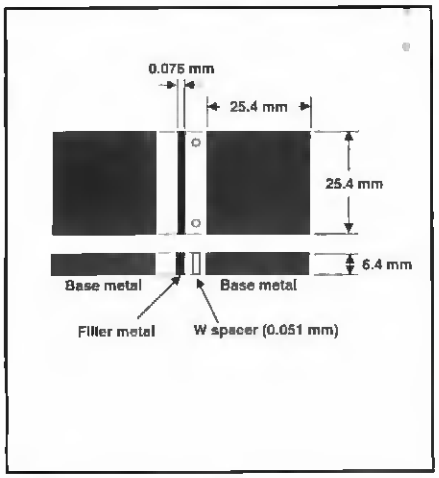

Fig. 1 — Configurations of the test specimen.

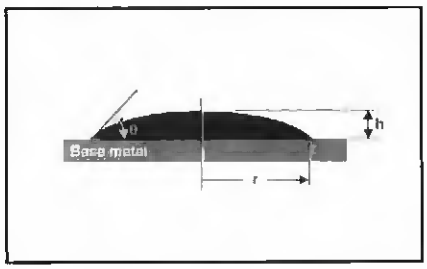

Fig. 2 — Schematic diagram of the sessile drop test specimen used to assess filler metal wetting and spreading. The quantitative metric is the contact angle, θ. The symbol r is the effective spread radius assuming a circular footprint to the area of spread, and h is the height of the filler metal mound.

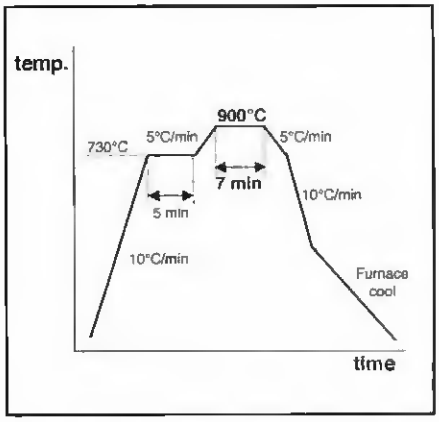

Fig. 3 — Time and temperature parameters for the Ag-Cu-Ti brazing process.

Table 1 — Arithmetic Average Roughness (RA) of the Base Metal Specimens with a √32 Finish

Base Metal	Condition	RA (μm)
Thermo-Span™	Solution treated	0.19 ± 0.02
Thermo-Span™	Solution treated and aged	0.09 ± 0.02
Inconel™ 718	As-received	0.12 ± 0.03
Inconel™ 718	Solution treated and aged	0.034 ± 0.005

Note: Surface Profilometry Data (Med. Scan Speed)

lidification process (Refs. 9–11). While in service, the brazed joint can be exposed to elevated temperatures over a long operating time, causing potential phase changes in the joint and, in particular, at the interface between the base and filler metals. The properties of the interface reaction products can significantly affect joint performance.

The long-term aging of brazed joints has not been extensively studied. Shimoo *et al.*, assessed the kinetics of solid-state reactions between Si_3N_4 and Ni (Ref. 12). Most aging studies have examined the interface microstructure that develops initially between the molten filler metal and the base metal during the brazing process (Refs. 13–15). Several publications describe high-temperature, interface reactions due to diffusion bonding processes (Refs. 16–18). Although the latter investigations provided important insights into potential solid-state reactions, the starting microstructures and aging conditions did not adequately represent those of brazed joints. The objective of the present investigation was to study filler metal/base metal interactions that can occur in the brazements of heat engines. The investigation examined brazed joints made between a low-temperature Ag-Cu-Ti filler metal and Thermo-Span™ or Inconel™ 718 substrate alloys; data from an analogous investigation of a high-melting-temperature Au-Ni-Ti braze alloy and Thermo-Span™, as well as an AISI Type 347 stainless steel, will be reported in Part 2. Standard analytical tools were used to characterize the brazed joint microstructures. The four-point bend test was used to determine the effect of microstructure on joint mechanical performance.

Experimental Procedures

Materials: Base Metals

The two base metals selected for this study were the precipitation-hardened Thermo-Span™ (24.5Ni-29.0Co-5.5Cr-4.8Nb-(Si, Ti, Al)-bal. Fe wt-%) and Inconel™ 718 (55Ni-21Cr-5.5 (Nb+Ti)-3.3Mo-bal. Fe alloys (Refs. 19, 20). The Thermo-Span™ was received in the solution-annealed condition [1093°C (2000°F), 1 h, air cool]; the condition of the as-received Inconel™ 718 stock was not documented. In order to assure consistent material properties, the Inconel™ 718 alloy was subjected to a solution annealing treatment. The Thermo-Span™ and Inconel™ 718 materials were then exposed to an aging (precipitation-anneal) heat treatment. The condition of each base metal was assessed using Rockwell C (HR_C) hardness measurements. Six measurements were performed on three sample blanks. The heat treatment schedules and hardness data follow.

Thermo-Span™ (As-received HR_C = 23±2, solution annealed). Solution annealing (at the mill): hold at 1093°C (2000°F) for 1 h; air cooling. Precipitation annealing: holding at 718°C (1324°F) for 8 h; furnace cooling at 0.015°C/s (0.027°F/s) to 621°C (1150°F); hold at 621°C (1150°F) for 8 h; air cooling. Postheat treatment $HR_C = 39±1$.

Inconel™ 718 (as-received HR_C = 22.5±0.5, unknown condition). Solution annealing: hold at 954° to 1010°C (1750° to 1850°F) for 0.5 to 1 h, air cooling. Precipitation annealing: hold at 718°C (1324°F) for 8 h, furnace cooling to 621°C (1150°F), holding for 10 h, air cooling. Postheat treatment $HR_C = 42±2$.

All brazing experiments were performed on base alloy surfaces that had been ground to a nominal √32 finish as determined by profilometer measurements. Four profilometer traces, two in one direction and the other two in a perpendicular direction, were made over a distance of 6 mm on each of duplicate samples. The arithmetic average roughness, or RA numbers (mean and ± one standard deviation) are shown in Table 1. The solution and aging heat treatments caused both substrate materials to have a lower surface roughness after grinding as compared to that of the as-received material.

Materials: Brazing Filler Metals

The brazing filler metal Cusil™ ABA (63.3Ag-35.1Cu-1.6Ti) was evaluated in this study (Ref. 21). The filler metal was in the form of 0.051-mm-thick (0.002-in.) strip. The Ag-Cu-Ti alloy has a nominal melting range of 780° to 815°C (1436° to 1499°F). The composition of the material batch used in this study was verified by atomic emission spectroscopy (AES); the chemical composition was 61.8±4.2 Cu, 35.1± 0.7 Ag, and 1.7 Ti (wt-%). The chemical analysis was performed in triplicate; the error terms represent a 95% confidence interval. The onset (solidus) temperature of the Ag-Cu-Ti alloy was

measured by differential thermal analysis (DTA). The DTA specimen was initially preconditioned by melting it with a heating ramp from 25° to 1100°C (77° to 2012°F) at a rate of 10°C/min (18°F/min). The sample was then cooled. A second heating cycle, which was performed on the same sample but at a ramp rate of 5°C/min (9°F/min), provided the actual data. For the Ag-Cu-Ti filler metal, a solidus temperature of 774°C (1425°F) was recorded as the average of two tests. This value is close to the nominal solidus temperature of 780°C (1436°F) cited by the manufacturer.

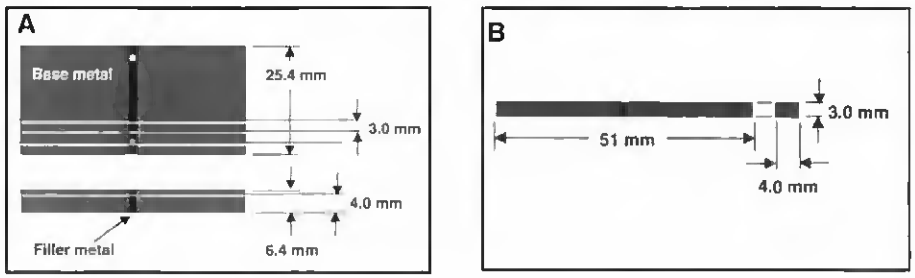

Fig. 4 — A — Schematic diagram showing the cutting of the test specimens from the brazed parent blocks; B — dimensions of the four-point bend specimens used in the mechanical testing and microstructural analyses.

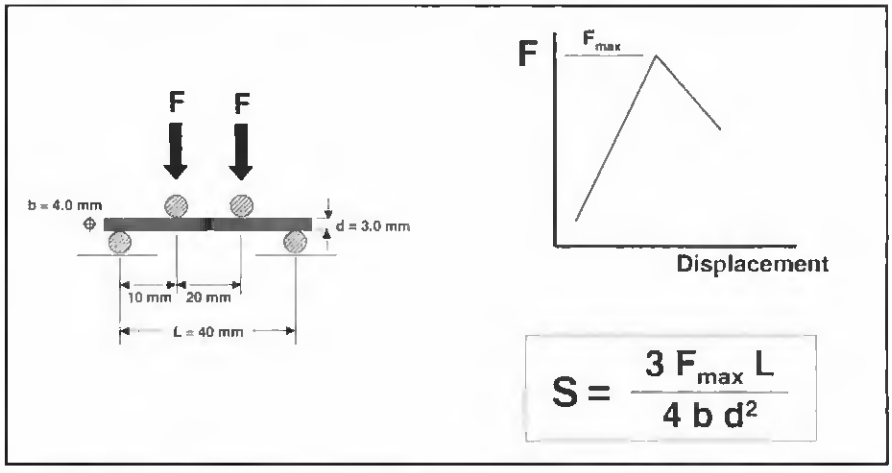

Fig. 5 — Schematic diagram of the four-point bend test procedure per MIL-STD-1942A. The flexure strength, S, was computed from the sample geometry and the maximum force, F.

'Parent' Block, Brazed Joint Assembly

The test specimen configuration used to evaluate the brazed joint microstructures, and from which the mechanical strength test pieces were fabricated, is shown in Fig. 1. The "parent" block of each alloy measured 25.4 x 25.4 x 6.4 mm (1.0 x 1.0 x 0.25 in.). Two parent blocks were joined along a 25.4-x 6.4-mm (1.0-x 0.25-in.) face that was ground to a nominal √32 finish. A preform of filler metal measuring 25.4 x 6.4 mm (1.0 x 0.25 in.) was preplaced between the two parent block surfaces. Control of the joint clearance was provided by the preplacement of two 0.051-mm-diameter (0.002-in.) tungsten (W) wires in the clearance. The parent blocks, W wires, and filler metal foil were stacked within a graphite fixture that maintained their alignment during the furnace brazing process. A weight was placed on top of the stack to assure formation of the target joint clearance thickness.

Brazing Process

An extensive development effort was conducted to determine suitable brazing process parameters. First, an assessment was made of the impact of brazing time and temperature on wetting and joint structure using an Inconel™ 718 alloy specimen. The furnace cycle was replicated five times. The furnace brazing process using the Ag-Cu-Ti filler alloy was performed under a 1.3-Pa (10-mtorr) partial pressure, flowing argon to prevent oxidation of titanium and to limit the loss of the higher vapor pressure silver constituent. The argon flow was begun once the sample temperature had reached 600°C (1112°F).

As a result of the preliminary evaluations, the nominal conditions for Ag-Cu-Ti filler metal brazing were set at a peak temperature of 830°C (1526°F) and duration of 7 min. The measured furnace cycle parameters were 830±1°C (1526±2°F) and 8.0±0.7 min, respectively.

Sessile drop (area-of-spread) experiments were performed in order to assess the sensitivity of the braze alloy wetting-and-spreading behavior to the peak temperature and time process parameters. These measurements were performed on postsolidified filler metal following removal of the sample from the furnace. The parameter for assessing wetting/spreading was the calculated contact angle, θ, that formed at the droplet front — Fig. 2. The value of θ was calculated from the volume, V, of filler metal used to make the drop and the physical dimensions of the drop. Observing that the sessile drops were approximately circular, an effective radius, r, of the footprint area was calculated from the image. Next, it was assumed the sessile drops formed a spherical cap. Therefore, the maximum height, h, of the droplet was calculated using the data and Equation 1 below

$$h = \{[(3V/\pi)^2 + r^6]^{1/2} + 3V/\pi\}^{1/3} - \{[(3V/\pi)^2 + r^6]^{1/2} - 3V/\pi\}^{1/3} \quad (1)$$

The contact angle was then calculated using Equation 2, which follows

$$\theta = \tan^{-1}[2rh/(r^2 - h^2)] \quad (2)$$

The values of the contact angles for each of the two base metals and peak process temperature combinations are given in Table 2. The low contact angles indicate excellent wetting/spreading by the braze alloys on the substrate materials. The reduced data scatter indicated the Ag-Cu-Ti alloy was relatively insensitive to the brazing temperature in the range of 830° to 850°C (1526° to 1562°F), using a 7-min processing time.

The effect of brazing time was of particular concern with the Ag-Cu-Ti filler metal based upon ancillary studies. Therefore, experiments were conducted in which the brazability of the Ag-Cu-Ti alloy was examined on Thermo-Span™, Inconel™ 718, and Type 347 stainless steel base metals. The brazing temperature for these experiments was 850°C (1562°F), while the brazing time was varied at 2, 7, 15, 30, and 60 min. The results of a qualitative evaluation appear in Table 3. It is apparent the wetting/spreading performance by the Ag-Cu-Ti filler metal on the selected base metals degraded when the time duration was reduced from 7 to 2 min. Therefore, instead of lengthening the time to 15 min, an alternative approach was to raise the peak temperature to 900°C

Table 2 — Sessile Drop Contact Angle Data Brazing Peak Temperature Analysis

Base Metal	Material Condition	Contact Angle Values (°) Ag-Cu-Ti 830°C (1526°F)	850°C (1562°F)
Thermo-Span™	Solution treated	—	—
Thermo-Span™	Solution treated and aged	3.6	4.2 (0.2)
Inconel™ 718	As-received	3.4	3.0
Inconel™ 718	Solution treated and aged	—	4.6 (1.1)
Type 347	As-received	4.4	6.5

Note: ± one standard deviation.

Table 3 — Qualitative Assessment of Brazability of Ag-Cu-Ti Filler Metal on Base Metals

Brazing Time (min)	Base Metals Thermo-span™	Inconel™ 718	Type 347 SS
2	poor	satisfactory	poor (dewet.)
7	satisfactory	excellent	excellent
15	very good	excellent	excellent
30	excellent	excellent	excellent
60	excellent	excellent	excellent

Note: Brazing temperature at 850°C (1562°F).

Table 4 — Mean Concentration and Scatter of the Sublayers

Sublayer No. 1 (at.-%) Si	Ti	Cr	Fe	Co	Ni	Cu	Nb	Ag
0.6 (0.2)	19 (2)	4.4 (0.6)	28 (4)	19 (2)	7 (1)	6 (3)	4 (2)	12 (10)
Sublayer No. 2 (at.-%) Si	**Ti**	**Cr**	**Fe**	**Co**	**Ni**	**Cu**	**Nb**	**Ag**
0.3 (0.2)	21 (4)	4.5 (0.4)	27 (3)	20 (3)	11 (5)	8 (7)	1.1 (0.8)	7 (4)

Note: Scatter is in parentheses.

(1652°F). The 900°C (1652°F), 7-min brazing conditions produced excellent results.

The selected time/temperature brazing profile for the Ag-Cu-Ti filler metal is illustrated in Fig. 3. The process began with a temperature rise of 10°C/min (18°F/min), to a subsolidus temperature of 730°C (1346°F) with a 5-min hold time. The temperature was then raised at 5°C/min (9°F/min) to the peak brazing value. Brazing was performed at 900°C (1652°F) for 7 min. The sample temperature was then slowly ramped down at 5°C/min (9°F/min) through the filler metal solidus temperature to the previous hold value of 730°C (1346°F). The cooling rate was then increased to 10°C/min (18°F/min) until a temperature of approximately 400°C (752°F) was reached, after which the assembly was allowed to cool at a rate of <10°C/min (18°F/min) to room temperature.

It is important to note the selected brazing cycle for the Ag-Cu-Ti filler metal overlapped the precipitation annealing conditions of both Thermo-Span™ and the Inconel™ 718 base metals. Consequently, in the event the brazing process was performed after precipitation annealing, an overaging condition could arise in base metals resulting in changes to their respective mechanical properties.

Microstructural Analysis of Sessile Drop Samples

Sessile drop samples were used in some assessments of the interface reactions in the aged couples. The aged samples were evaluated using optical microscopy, scanning electron microscopy (SEM), and electron microprobe analysis (EMPA) techniques.

Mechanical Test Specimen Fabrication

Mechanical strength measurements were performed on individual specimens that were cut from the brazed parent blocks. Shown in Fig. 4A is a schematic diagram illustrating the manner in which the test specimens were cut from the brazed parent blocks. The cuts produced seven test pieces having a width that was ground to a dimension of 3.0 mm (0.12 in.). Only those five pieces originating from the center portion of the parent block assembly were used so as to avoid the tungsten spacer wire. The final dimensions of the test specimens (Fig. 4B) were reached by a grinding operation that reduced the original "thickness dimension" from 6.4 to 4.0 mm (0.25 to 0.16 in.). The sample geometry complied with MIL-STD-1942A, *Flexure Strength of High Performance Ceramics at Ambient Temperature.* Four of the five test samples were used for the mechanical tests. The remaining sample was cross sectioned and its microstructure analyzed to supplement data obtained from the sessile drop samples.

Bend strength specimens were successfully constructed from Thermo-Span™ or Inconel™ 718 and the Ag-Cu-Ti filler metal. An attempt to construct specimens with the Type 347 stainless steel base metal and Ag-Cu-Ti filler metal was unsuccessful. The specimens simply fell apart during the cutting operations used to obtain the final sample geometry. No further investigation was performed to determine the cause of the weakened joints.

Four-Point Bend Mechanical Strength Test Procedure

The four-point bend test setup (per MIL-STD-1942A) is shown in Fig. 5. The test specimen was placed on top of two outer support rollers that were separated by a distance of 40 mm; the ground surface was in contact with the rollers. The two inner or "loading" rollers that were separated by a distance of 20 mm (0.79 in.) were positioned on top of the specimen. No significant preload was applied prior to the start of testing. The specimen was subjected to a constant cross head displacement rate of 8.3×10^{-3} mm/s (3.3×10^{-4} in./s). The flexure strength, S, was computed according to the following equation:

$$S = \frac{3F_{max}L}{4\,b\,d^2} \qquad (3)$$

where F_{max} is the maximum force (load); L is support roller span of 40 mm (1.6 in.); b is the specimen width of 4.0 mm (0.16 in.); and d is the specimen thickness of 3.0

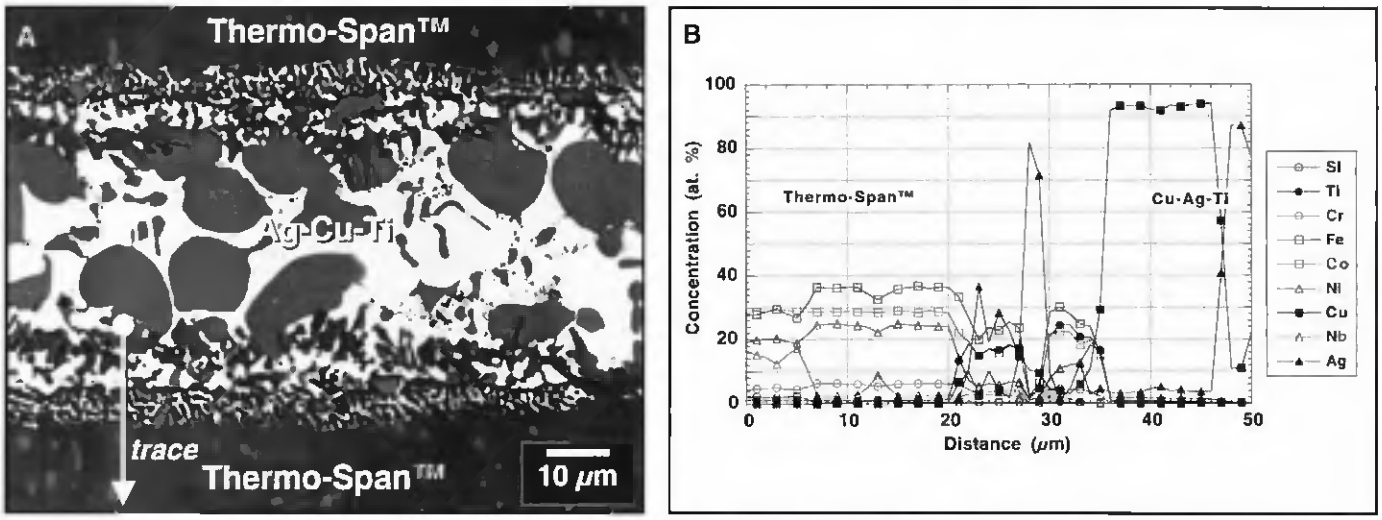

Fig. 6 — A — SEM micrograph of the as-fabricated, Ag-Cu-Ti/Thermo-Span™ joint; B — representative EMPA trace across the interface between the Thermo-Span™ base metal and the Ag-Cu-Ti filler metal in the as-fabricated condition.

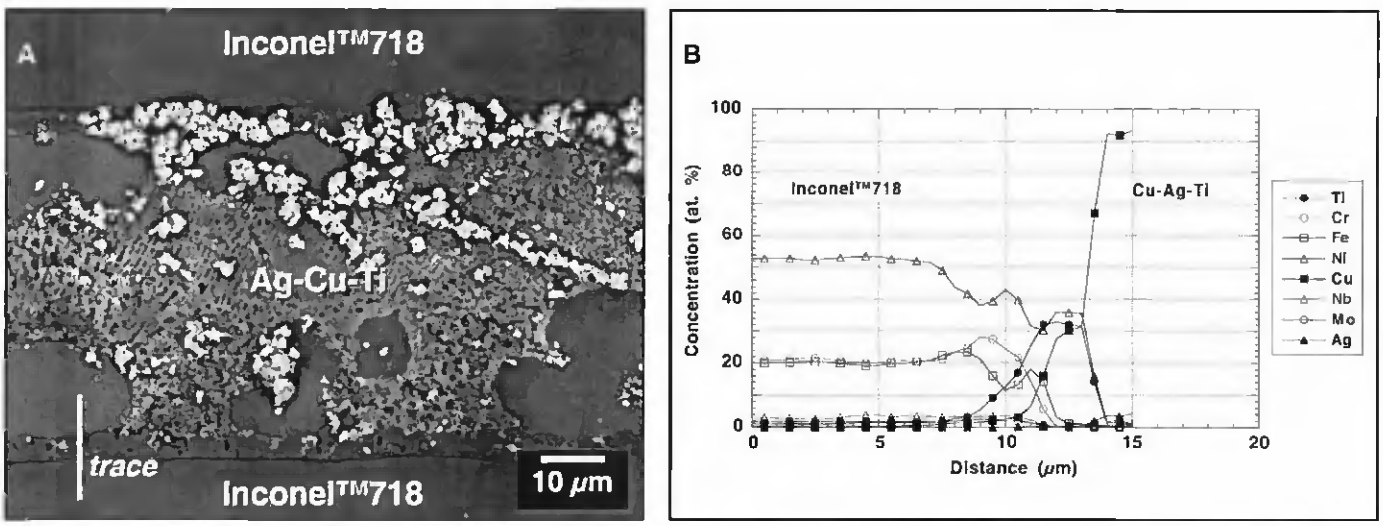

Fig. 7 — A — SEM micrograph; B — representative EMPA trace across the interface between the Inconel™ 718 base metal and the Ag-Cu-Ti filler metal in the as-fabricated condition.

mm (0.12 in.). The strength data were represented by the mean and the standard deviation of the multiple tests.

Aging Environments

The aging treatments were performed at temperatures of 150°C (302°F), 350°C (662°F), and 575°C (1067°F) and time periods of 100, 200, and 300 days. The specimen was placed in a quartz ampoule along with a piece of Ta foil. The ampoule was then backfilled with Ar at 10-mtorr (1.3-Pa) pressure and sealed. The Ta foil served as a getter for residual O_2. Sessile drop specimens were fabricated to evaluate microstructural changes due to these aging treatments.

A more limited range of aging parameters was used for the four-point bend specimens. Those aging conditions were temperatures of 350°C (662°F) and 575°C (1067°F) and time durations of 100 and 200 days.

Results and Discussion

Sessile Drop Morphology from the Wetting/Spreading Experiments

The process development experiments did not reveal any distinguishable features accompanying the wetting/spreading behavior of the Ag-Cu-Ti alloy.

Brazed Joint Microstructure: As-Fabricated Condition

The composition of the Thermo-Span™ base metal/Ag-Cu-Ti filler metal interface was examined by electron microprobe analysis (EMPA). An SEM micrograph and representative EMPA trace taken from the five scans made across the interface are shown in Fig. 6A and B, respectively. The interface structure was comprised of two sublayers. The first sublayer, termed No. 1, was centered approximately at the 24-μm position in Fig. 6B, between the base metal and a Ag-rich layer. Sublayer No. 1 had a nominal thickness of about 8 μm (3 x 10^{-4} in.). The second sublayer, termed No. 2, was centered approximately at the 31-μm (0.0012-in.) position in Fig. 6B, between the Ag-rich layer and the filler metal. Sublayer No. 2 had a nominal thickness of approximately 5 μm (2 x 10^{-4} in.).

A composition (at.-%) was determined for each of the two sublayers. The composition value was determined from element levels that were measured at the midpoint of that sublayer. The mean concentration and a scatter term in parentheses that was

Table 5 — Mean Compositions and Standard Deviation of the Sublayers

Sublayer No. 1 (at.-%)							
Ti	Cr	Fe	Ni	Cu	Nb	Mo	Ag
19 (2)	19 (2)	15 (3)	37 (3)	5 (2)	3.1 (0.5)	1.7 (0.2)	0.1 (0.2)
Sublayer No. 2 (at.-%)							
Ti	Cr	Fe	Ni	Cu	Nb	Mo	Ag
31 (2)	0.2 (0.3)	3 (2)	33 (3)	32 (4)	0.2 (0.4)	0 (0)	2 (4)

Note: Standard deviation is in parentheses.

± one standard deviation are shown in Table 4.

Specific compositions were derived from the binary phase diagrams of pairwise element combinations. First, sublayer No. 1 was examined. It was assumed iron, nickel, and cobalt would combine as a single, pseudo-element based upon the mutual solubility of these transition elements over a wide composition-temperature range (Ref. 22). Next, the roles of copper and niobium were assessed. First, copper exhibits complete solid solubility with nickel but nearly complete insolubility with iron and cobalt (Ref. 23). Also, copper forms an extensive series of compounds having narrow composition ranges when combined with titanium (Ref. 24). Therefore, it was assumed copper would join iron, nickel, and cobalt as the pseudo-element (Fe, Ni, Co, Cu). Niobium forms compounds of limited composition range with iron, nickel, and cobalt, but has complete solid solubility with titanium over an extensive area of the phase diagram (Ref. 25). Thus, it was surmised niobium would join with titanium as the pseudo-element, (Ti, Nb).

It was more difficult to hypothesize the behaviors of the other three elements, silicon (0.6 at.-%), chromium (4.4 at.-%), and silver (12 at.-%). It was assumed the chromium and silicon atoms would behave like titanium and niobium because of their similar refractory natures. Silver would form a separate constituent because there was no obvious interaction between it and the other elements or pseudo-elements.

The above analyses resulted in a two-phase composition for sublayer No. 1. The first phase had the approximate formula $(Fe, Ni, Co, Cu)_2(Nb, Ti, Si, Cr)$; the second phase was Ag. The volume fraction of the two phases was nine to one, respectively.

A similar analysis performed on sublayer No. 2 showed it to have the same composition as sublayer No. 1, given the experimental error.

The EMPA analysis showed an accumulation of titanium at the base metal/filler metal interface. A driving force for the titanium buildup may have been the oxide layer on the Thermo-Span™ surface. Oxides of the metal constituents, nickel, cobalt, chromium, niobium, silicon, and aluminum may have contributed to the driving force for titanium to diffuse to the interface.

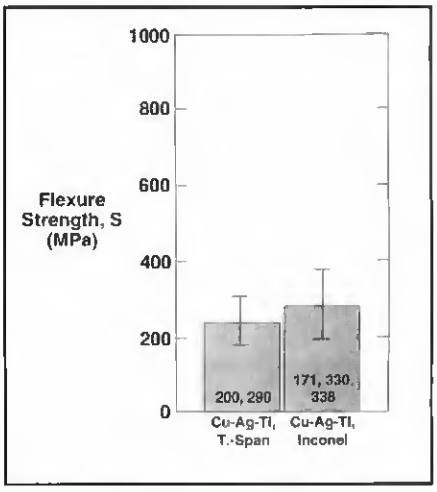

Fig. 8 — Bar graph showing the four-point bend strengths of the as-fabricated joints for both base metal/Ag-Cu-Ti filler metal combinations. The length of the bars is equal to the mean; the individual test values are included within each bar graphic.

Electron microprobe analysis scans were also performed within the Thermo-Span™ base metal, parallel to the base metal/filler metal interface, at distances of approximately 10 μm (3.9×10^{-4} in.) and 25 μm (9.8×10^{-4} in.) away from that interface. The purpose of this analysis was to identify bulk and/or grain boundary transport mechanisms by the molten filler metal. The filler metal elements copper, silver, and titanium were observed in the Thermo-Span™ grain boundaries at the 10 μm (3.9×10^{-4} in.) distance from the interface. However, the EMPA trace at 25 μm

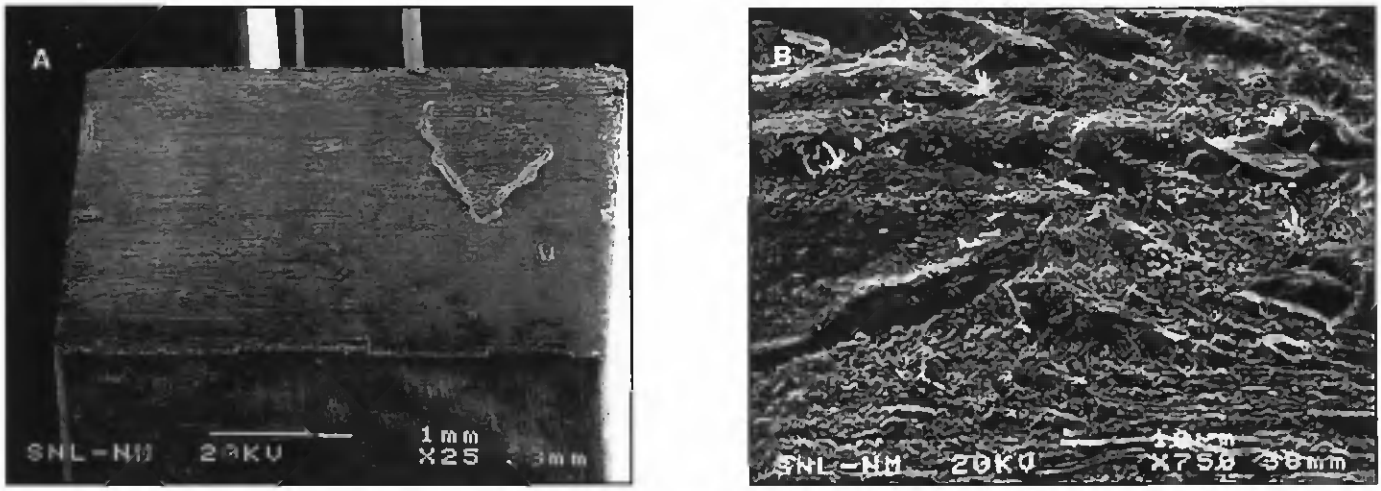

Fig. 9 — Low-magnification (A) and high-magnification (B) scanning electron micrographs showing the fracture surface of the Thermo-Span™ test specimens made with the Ag-Cu-Ti filler metal representing the as-fabricated condition.

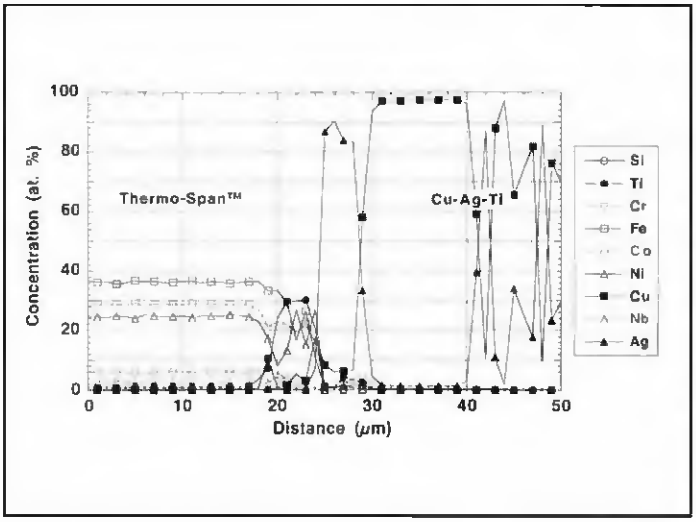

Fig. 10 — Representative EMPA trace of the Thermo-Span™/Ag-Cu-Ti brazed joint after aging at 575°C (1067°F) for 300 days.

(9.8 x 10^{-4} in.) revealed only the constituents of the Thermo-Span™ alloy.

The microstructure of the interface formed by the Inconel™ 718 base metal and the Ag-Cu-Ti filler metal was examined. An SEM micrograph and representative EMPA trace from this couple are shown in Fig. 7A and B, respectively. Two sublayers were identified. Sublayer No. 1 was located next to the substrate and sublayer No. 2 was situated next to the filler metal field. The two sublayers were separated by a small iron peak. Sublayer No. 1 was approximately 2 μm (7.9 x 10^{-5} in.) thick; sublayer No. 2 was 2 to 3 μm (7.9 x 10^{-5} in. to 1.2 x 10^{-4} in.) thick. The mean compositions and standard deviation in parentheses for the two layers are presented in Table 5.

The layer compositions were developed in a manner similar to that used for the Thermo-Span™ base metal. Sublayer No. 1 had the composition $(Fe,Ni,Cu)_3(Ti,Cr,Nb,Mo)_2$. Sublayer No. 2 had the composition $(Fe,Ni,Cu)_2(Ti,Cr,Nb,Mo)$. It was observed silver was present in small quantities in both sublayers (<1% and 2%, respectively). The oxide layer present on the Inconel™ 718 surface probably provided some driving force for titanium segregation in the vicinity of the base metal/filler metal interface.

Four-Point Bending Strength: As-Fabricated Condition

The four-point bend strength data are shown in Fig. 8. The individual test values are included within the bar chart. Similar mean strength values were observed for brazed joints made with either Thermo-Span™ or Inconel™ 718 base metals; those strengths were 250±60 MPa (36±9 ksi) and 280±90 MPa (41±13 MPa), respectively. There was no deformation observed in either the Thermo-Span™ or Inconel™ 718 bend bars after testing to indicate the yield strengths of either base metal had been exceeded.

Shown in Fig. 9 are low- and high-magnification SEM photographs of the fracture surfaces of an as-fabricated, Thermo-Span™/Ag-Cu-Ti test specimen. The low magnification images indicated the failure path progressed along the interface between the filler metal and the base metal. This hypothesis was substantiated by an energy dispersive X-ray analysis (EDXA) evaluation of the fracture surface, which revealed a relatively strong titanium presence. The Thermo-Span™ base metal contains titanium, but only at a level of 0.8%, which is too low to have accounted for the observed peak intensity. In addition, the earlier EDXA presented in Fig. 6 showed the accumulation of titanium at the base metal/filler metal interface, lending further evidence the fracture path was lo-

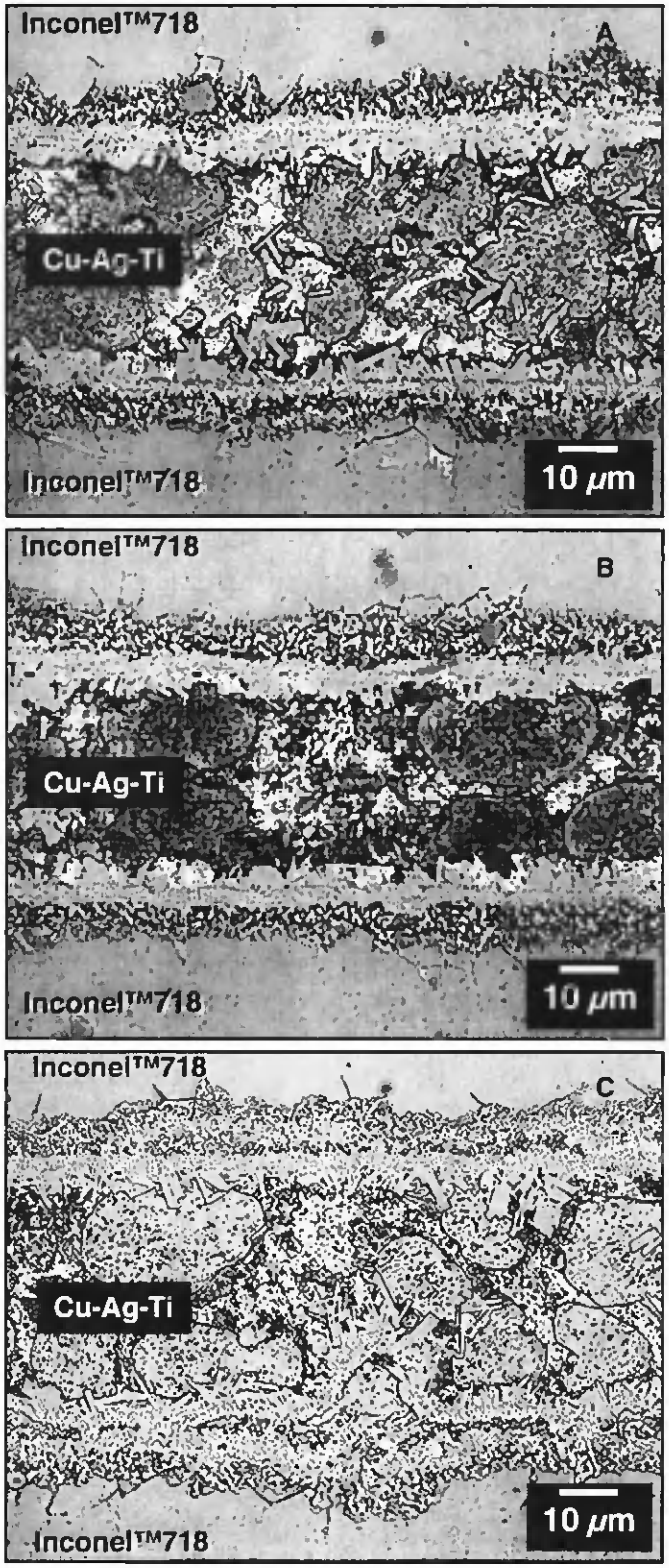

Fig. 11 — Optical micrographs of cross sections of the Inconel™ 718/Ag-Cu-Ti brazed joints following aging for 200 days at various temperatures. A — 150°C (302°F); B — 350°C (662°F); C — 575°C (1067°F).

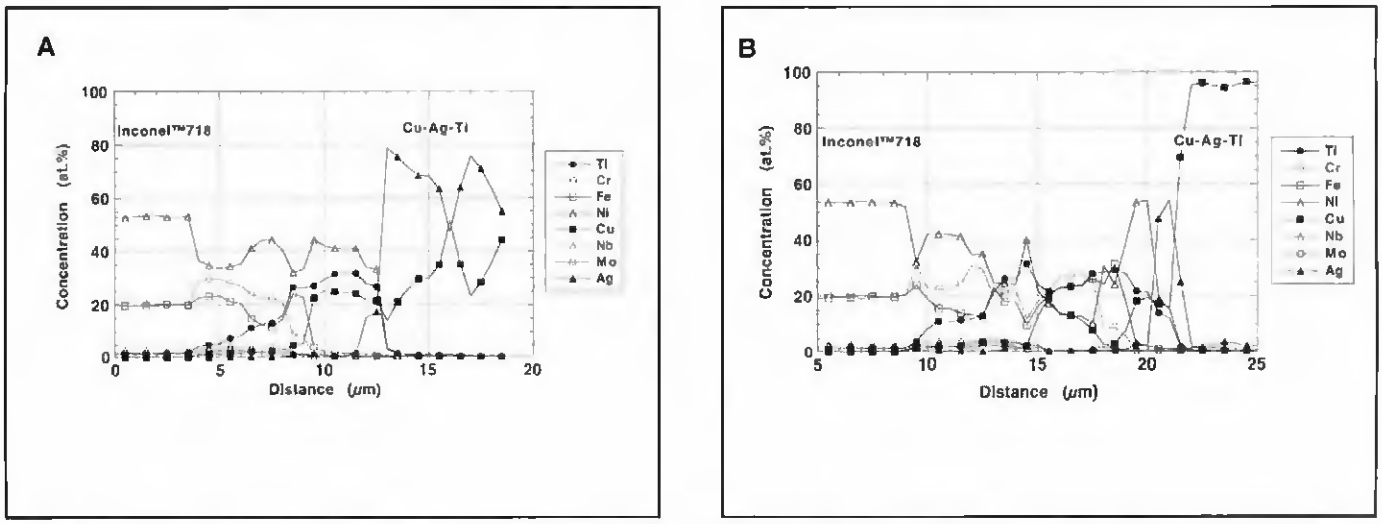

Fig. 12 — EMPA traces for the Inconel™ 718/Ag-Cu-Ti brazed joints. A — After aging at 150°C (302°F) for 100 days; B — after aging at 575°C (1067°F) for 300 days.

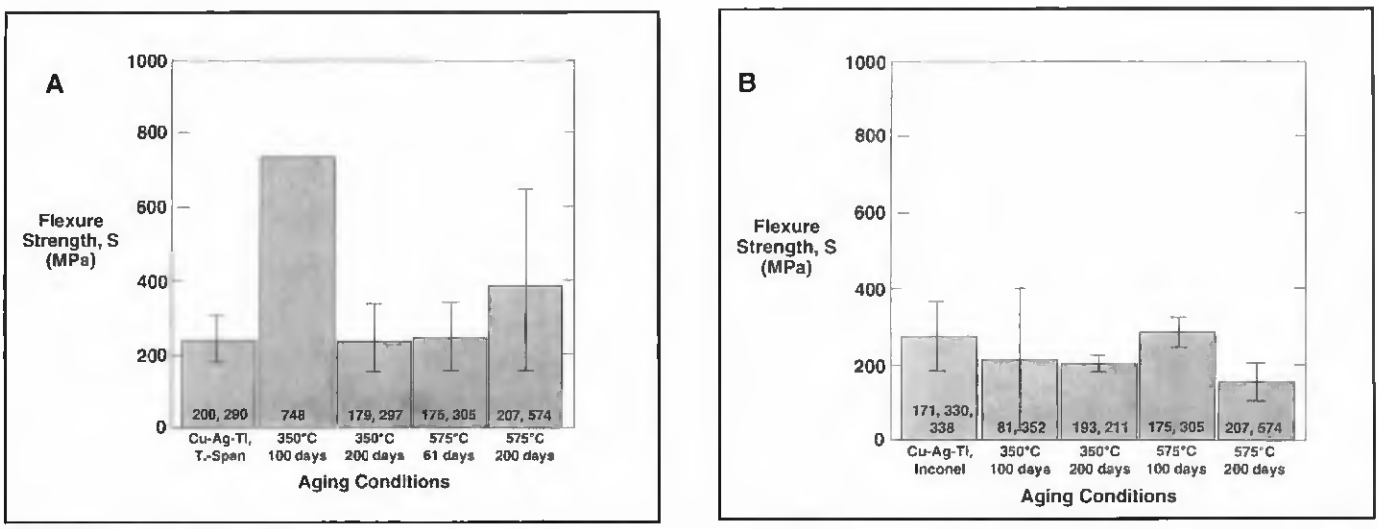

Fig. 13 — A — Bar chart of mean strength values for the aged Thermo-Span™/Ag-Cu-Ti brazed joints; B — bar chart of mean strength values for the aged Inconel™ 718/Ag-Cu-Ti brazed joints.

cated along the base metal/filler metal interface. The high magnification SEM images showed small hillock-like features on the fracture surface.

A similar fracture surface morphology and presence of titanium were observed with the tested Inconel™ 718/Ag-Cu-Ti specimens, indicating a crack path was along the base metal/filler metal interface.

Brazed Joint Microstructure: Post-Aging Condition

Optical microscopy of metallographic cross sections was used to identify aging-related changes to the microstructure of the Thermo-Span™/Ag-Cu-Ti brazed joints. Very little difference was observed in the interface microstructures between the different aging treatments. A representative EMPA trace of a Thermo-Span™ brazed joint aged at 575°C (1067°F) for 300 days is shown in Fig. 10. The EMPA trace from an as-fabricated sample is shown in Fig. 6B. The thickness of the total reaction layer after aging was approximately 8 μm (3 x 10^{-4} in.), indicating a decrease of 40% as compared to the as-fabricated case. The composition of the reaction layer was determined to be $(Fe,Ni,Co,Cu)_2(Ti,Nb,Si,Cr)$, which was identical to the reaction layer compositions determined for the as-fabricated sublayers Nos. 1 and 2; however, unlike the as-fabricated sublayer No. 1, silver was not present to a significant degree (0.4±0.6%).

Electron microprobe analysis traces were made in the Thermo-Span™ base metal of the specimen aged at 150°C (302°F) for 200 days. Scans were made parallel to the filler metal/base metal interface, at distances of 10 μm (3.9 x 10^{-4} in.) and 25 μm (9.8 x 10^{-4} in.). In neither instance was there evidence that accelerated diffusion into, nor reaction of, the Thermo-Span™ base metal had occurred.

The aged Ag-Cu-Ti joints made with Inconel™ 718 base metal were similarly analyzed. Shown in Fig. 11 is a sequence of cross-section micrographs from specimens aged for 200 days at temperatures of 150°C (302°F), 350°C (662°F), and 575°C (1067°F). The interface reaction layers grew thicker by growing further into the base metal. Grain boundary diffusion/reaction artifacts, originally observed in the as-fabricated specimen, were retained. The formation of blocky particles located at the interface between the reaction layer and the filler metal increased with aging temperature. Finally, in the filler metal, the Cu-rich phase size was not significantly affected by the aging treatment.

Electron microprobe analysis was performed across the Inconel™ 718/Ag-Cu-

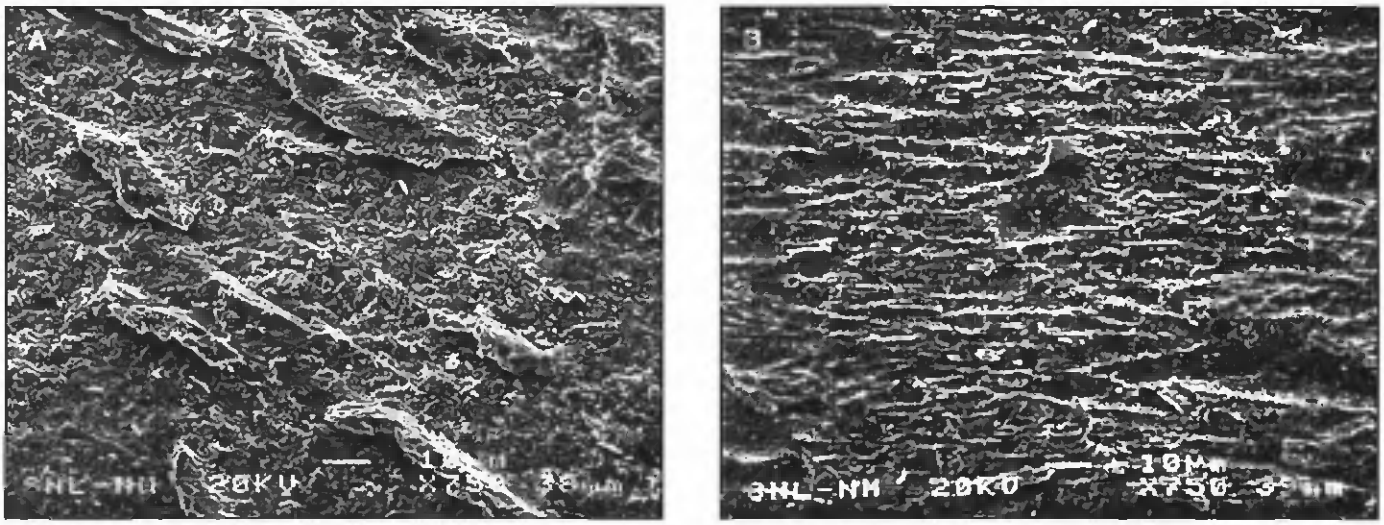

Fig. 14 — SEM micrographs of the fracture surfaces of Thermo-Span™/Ag-Cu-Ti bend bars aged at different temperatures. A — 350°C (662°F) for 100 days; B — 575°C (1067°F) for 200 days.

Ti interface of aged brazed joints. Representative EMPA traces are provided in Fig. 12 for the aging conditions of 150°C (302°F) for 100 days and 575°C (1067°F) for 300 days. Recall that the interface of the as-fabricated condition (Fig. 7B) was comprised of two sublayers, each approximately 2 to 3 μm (7.9×10^{-5} in. to 1.2×10^{-4} in.) thick and separated by a narrow band having a high concentration of iron. Aging at 150°C (302°F) for 100 days resulted in the following changes: There was a slight thickening of both sublayers to values of approximately 3 to 5 μm (1.2 to 2.0×10^{-4} in.). The intensity of the iron peak separating the two sublayers grew slightly. The midpoint composition of sublayer No. 1 (located next to the base metal) was unchanged when compared to the as-fabricated condition ($(Fe,Ni,Cu)_3(Ti,Cr,Nb,Mo)_2$). The sub-layer No. 2 composition changed from $(Fe,Ni,Cu)_2(Ti,Cr,Nb,Mo)$ to $(Fe,Ni,Cu)_7(Ti,Cr,Nb,Mo)_3$ after aging.

The aged sublayer No. 2 also exhibited an increased level of titanium, as well as significant spatial fluctuations in the chromium, iron, and copper concentrations. In fact, for two of the five EMPA traces, the chromium and iron concentrations increased to an average of 14% and 22%, respectively, and the copper concentration dropped to approximately 3%, resulting in a composition of $(Fe,Ni,Cu)_3(Ti,Cr,Nb,Mo)_2$, which resembled that of sublayer No. 1.

Aging the Inconel™ 718/Ag-Cu-Ti specimens at 575°C (1067°F) for 300 days (Fig. 12B) caused the interface reaction layer thickness to grow to 22 μm (8.7×10^{-4} in.). Two sublayer compositions were identified from the EMPA traces, both having compositions similar to those observed after aging for 100 days at 150°C (302°F): sublayer No. 1, $(Fe,Ni,Cu)_3(Ti,Cr,Nb,Mo)_2$ and sub-layer No.2, $(Fe,Ni,Cu)_7(Ti,Cr,Nb,Mo)_3$. Sublayer No. 2 exhibited locally higher concentrations of chromium (8–9%) and iron (25%) that were compensated by proportional decreases in the concentrations of other elements; the copper content remained the same for all five traces.

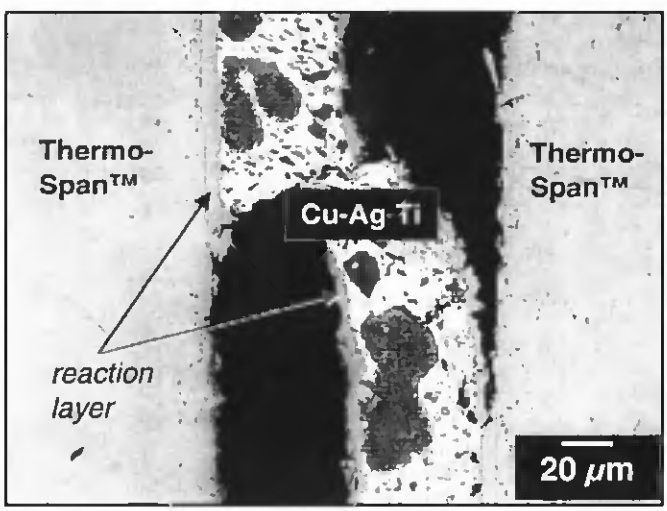

Fig. 15 — Optical micrograph of the fracture path in a Thermo-Span™/Ag-Cu-Ti specimen that was aged at 575°C (1067°F) for 200 days prior to testing.

In summary, the effect of aging treatments on Thermo-Span™/Ag-Cu-Ti braze joints was a slight decrease in the interface reaction zone thickness; there were no significant changes to the sublayer compositions. In the case of the Inconel™ 718/Ag-Cu-Ti specimens, aging treatments caused a noticeable increase in the thickness of the reaction layer. Aside from local chromium, iron, and copper fluctuations in the composition of the No. 2 sublayer, the sublayer compositions were similar to those recorded for the as-fabricated condition.

Four-Point Bending Strength: Post-Aging Condition

The four-point bend strength data from the aged Thermo-Span™/Ag-Cu-Ti and Inconel™ 718/Ag-Cu-Ti specimens appear in Fig. 13. The aging treatments did not appear to cause a significant change to the strength of the Thermo-Span™/Ag-Cu-Ti brazed joints — Fig. 13A. The possible exception was the single specimen aged at 350°C (662°F) for 100 days. The repeatability of this latter test was not confirmed.

The fracture surfaces of samples aged at 350°C (662°F) for 100 days and 575°C (1067°F) for 200 days were examined. At low magnification, the fracture surfaces appeared similar to those of the as-fabricated case (Fig. 9A) in which the fracture path was located near the filler metal/base metal interface. Shown in Fig. 14 are higher magnification SEM images of the fracture surfaces. The specimen aged at

350°C (662°F) for 100 days (Fig. 14A) had the same hillock features as did the fracture surface of the as-fabricated (Fig. 9B). Also, the aging treatment caused small peaks and valleys to appear on the fracture surface. The aging treatment at 575°C (1067°F) for 200 days caused the hillock structures to largely disappear; however, the fine peak and valley morphology remained on the fracture surfaces. Shown in Fig. 15 is the optical micrograph of the cross section of a tested bend bar that had been aged at 575°C (1067°F) for 200 days. The fracture path lay at the Thermo-Span™/Ag-Cu-Ti interface (as was similarly observed in the as-fabricated case). More specifically, however, the fracture path was observed to move between the reaction layer/Thermo-Span™ interface and the reaction layer/braze alloy interface. The scale of these fracture path jumps appeared to be commensurate with the fine scale peaks and valleys observed on the fracture surfaces.

The bend strength data aged Inconel™ 718/Ag-Cu-Ti specimens appear in Fig. 13B. As was the case with the Thermo-Span™/Ag-Cu-Ti couples, the aging treatments did not cause a significant change to the strength values. Similarly, the fracture paths were not changed from their base metal/filler metal interface.

In summary, the four-point bend strengths for both the Thermo-Span™ and Inconel™ 718 braze joints made with the Ag-Cu-Ti filler metal were not significantly affected by the aging treatments. The fracture paths remained located generally at the base metal/filler metal interface with only some minor differences being observed in the finer details of the fracture surfaces as a consequence of the aging treatments.

Summary

1) The effects of aging were examined for brazed joints made between the 63.3Ag-35.1Cu-1.6Ti filler metal and Thermo-Span™ and Inconel™ 718 base metals.

2) Excellent wetting and spreading was exhibited by the Ag-Cu-Ti filler metal on both base metals as determined by contact angle measurements.

3) The as-fabricated Thermo-Span™/Ag-Cu-Ti brazed joints exhibited two sublayers at the base metal/filler metal interface. Each sublayer contained (Fe, Ni, Co, Cu)$_2$(Nb, Ti, Si, Cr) and silver in a volume ratio of 9:1. The two sublayers were separated by a Ag-rich zone. Aging reduced the reaction zone to one sublayer having a composition of (Fe, Ni, Co, Cu)$_2$(Nb, Ti, Si, Cr). The thickness of this layer was less than the total reaction zone of the as-fabricated specimen.

4) The interface reaction zone in the as-fabricated Inconel™ 718/Ag-Cu-Ti specimens contained two sublayers. Sublayer No. 1, located next to the base metal, had the composition of $(Fe,Ni,Cu)_3(Ti,Cr,Nb,Mo)_2$. Sublayer No. 2, located next to the filler metal field, had the composition of $(Fe,Ni,Cu)_2(Ti,Cr,Nb,Mo)$. The composition of sublayer No. 1 remained unchanged after aging. The composition of sublayer No. 2 shifted to primarily $(Fe,Ni,Cu)_7(Ti,Cr,Nb,Mo)_3$, but with some localized variations along the interface. Aging caused growth of the overall interface reaction layer.

5) The four-point bend strengths observed with the as-fabricated Thermo-Span™/Ag-Cu-Ti and Inconel™ 718/Ag-Cu-Ti specimens were not significantly changed after each of the aging treatments. The fracture path remained located at the base metal/filler metal interface for as-fabricated as well as for aged test specimens.

Acknowledgments

The authors wish to thank A. Kilgo, who performed the metallographic sample preparation; P. Hlava, who performed the EMPA; and B. Ritchey for the SEM micrographs. The authors would also like to thank C. Robino for his very thorough review of the manuscript. Sandia is a multiprogram laboratory operated by Sandia Corporation, a Lockheed Martin Company, for the United States Dept. of Energy under contract DE-AC04-94AL85000.

References

1. Mangin, C., Neely, J., and Clark, J. 1993. The potential for advanced ceramics in automotive engine applications. *Journal of Metals* (6): 23–27.

2. DeLuca, M., and Swain, J. 1987. An advanced ceramic-to-metal joining process. *Ceramic Eng. Sci. Proc.* 8(7-8): 602–610.

3. Santella, M. 1993. Joining of ceramics for heat engine applications. Ceramic Tech. Project-Semiannual Prog. Rep., ORNL/TM-12428, pp. 167–180, Oak Ridge National Laboratory, Oak Ridge, Tenn.

4. Levy, A. 1991. Thermal residual stresses in ceramic-to-metal brazed joints. *J. Am. Ceramic Soc.* 74(9): 2141–2147.

5. Moorhead, A., and Hyoun, K. 1992. Joining oxide ceramics. *Engineered Materials Handbook*, Vol. 4, *Ceramics and Glasses*, pp. 511–522. Materials Park, Ohio: ASM International.

6. Santella, M. 1993. Ceramic-metal joining ceramic technology project, Semiannual progress report, 10/92–3/93: pp. 167–180. Oak Ridge, Tenn: National Laboratory.

7. Kovar™, Invar 36™, and Alloy 42™ are registered trademarks of Carpenter Technology Corp., Reading, Pa.

8. Harner, L. 1994. Selecting controlled expansion alloys. *Advanced Materials and Processes* October: 19–22.

9. Bex, W. 1989. Metallurgical study of superalloy brazing alloys. *Proc. Propulsion and Energetics Panel 72nd Specialists' Meeting*, Bath, U.K., pp. 27–12.

10. Sasabe, K. 1991. Effect of joint clearance on fatigue strength of brazed joint. *Trans. Nat. Res. Inst. For Metals* 33(1): 36–41.

11. Dicus, D., and Buckley, J. 1972. The effects of high-temperature brazing and thermal cycling on the mechanical properties of Hastelloy X. NASA Langley Research Center Report, L-8376, pp. 1–21.

12. Shimoo, T., Kobayashi, Y., and Okamura, K. 1992. Kinetics of reaction of Si_3N_4 with Ni. *Journal of the Ceramic Soc. of Japan*, International Edition 100, pp. 801–806.

13. Naka, M. 1992. Controlling of ceramic-metal interfacial structure using molten metals. *Trans. Weld. Res. Inst.* 21: 1–7.

14. Boadi, J., Yano, T., and Iseki, T. 1987. Brazing of pressureless-sintered SiC using Ag-Cu-Ti alloy. *Journal of Material. Sci.* 22: 2431–2434.

15. Bang, K., and Liu, S. 1994. Interfacial reaction between alumina and Cu-Ti filler metal during reactive metal brazing. *Welding Journal* 73(3): 54-s to 60-s.

16. Kodentsov, A., Kivilahti, J., and Loo, F. 1993. Interfaces in Si_3Ni_4/Ni-Cr alloy joints. *Ceramic Trans.* 35: 1–10.

17. Beraud, C., Courbiere, M., Esnour, C., Juve, D., and Treheux, D. 1989. Study of copper-alumina bonding. *J. Mater. Sci.* 24: 4545–4554.

18. Allen, R., and Borbidge, W. 1983. Solid state metal-ceramic bonding of platinum to alumina. *J. Mater. Sci.* 18: 2835–2843.

19. Thermo-Span™ is a registered trademark of Carpenter Technologies Corp., Reading, Pa.

20. Inconel™ is a registered trademark of Huntington Alloys, Huntington, W.Va.

21. Cusil™ is a registered trademark of WESGO Products.

22. *Binary Alloy Phase Diagrams*, Vol. 2, 1986. Ed. by T. Massalski, pp. 764, 783, 1086. Materials Park, Ohio: ASM International.

23. *ibid.* pp. 760, 916, and 942.

24. *ibid.* p. 971.

25. *ibid.* pp. 780, 1084, 1682, and 1704.